Final Report

Title: Aerodynamic Investigation of Smart Flying Wing MAV

AFOSR/AOARD Reference Number: FA2386-08-1-4088 and FA2386-09-1-4109

AFOSR/AOARD Program Manager: Lt. Col. Dr. John Seo, AOARD, Tokyo

Period of Performance: 2008-2010

Submission Date: 3rd November 2010

PI: Dr. Arnab Roy, Department of Aerospace Engineering,
Indian Institute of Technology Kharagpur, Pin-721302, India
CO-PI: Dr. Anup Ghosh, Department of Aerospace Engineering,
Indian Institute of Technology Kharagpur, Pin-721302, India

Report Documentation Page

Form Approved
OMB No. 0704-0188

1. REPORT DATE	2. REPORT TYPE	3. DATES COVERED
15 NOV 2010	**Final**	**24-07-2009 to 23-08-2010**

4. TITLE AND SUBTITLE
Aerodynamic Investigation of Smart Flying Wing MAV

5a. CONTRACT NUMBER
FA23860914109

5b. GRANT NUMBER

5c. PROGRAM ELEMENT NUMBER

6. AUTHOR(S)
Amab Roy

5d. PROJECT NUMBER

5e. TASK NUMBER

5f. WORK UNIT NUMBER

7. PERFORMING ORGANIZATION NAME(S) AND ADDRESS(ES)
Indian Institute of Technology Kharagpur,Indian Institute of Technology Kharagpur,Kharagpur, West Bengal 721302,India,NA,NA

8. PERFORMING ORGANIZATION REPORT NUMBER
N/A

9. SPONSORING/MONITORING AGENCY NAME(S) AND ADDRESS(ES)
AOARD, UNIT 45002, APO, AP, 96338-5002

10. SPONSOR/MONITOR'S ACRONYM(S)
AOARD

11. SPONSOR/MONITOR'S REPORT NUMBER(S)
AOARD-094109

12. DISTRIBUTION/AVAILABILITY STATEMENT
Approved for public release; distribution unlimited

13. SUPPLEMENTARY NOTES

14. ABSTRACT

The objectives of the present research include development of a suitable CFD solver for solving incompressible flow past airfoils suitable for flying wing micro air vehicle (MAV) design. Suitable airfoils would have to be selected for the purpose. This would be followed by development of a structural analysis solver that would structurally model the airfoil and integrate this solver with the flow solver in order to perform the fluid structure interaction studies for flexible airfoils. Compute flow past selected flexible airfoils and compare their aerodynamic and structural performance with corresponding rigid airfoils. Implementation of smart concept in the structure solver in order to improve the flexible airfoil performance. Perform the fluid structure interaction studies by incorporating smart active layer and explore whether such an embedded layer can improve the aerodynamic and/or structural behavior of the flexible airfoil. The studies are to be performed over a moderate range of Reynolds number and a fairly wide range of angles of attack to cover a reasonably wide variety of flow conditions. The scope of the project also includes flow solution past three dimensional finite wings with some optimization of the wing platform.

15. SUBJECT TERMS
Micro Air Vehicles (MAVs), Computational Aerodynamics, Computational Fluid Dynamics (CFD)

16. SECURITY CLASSIFICATION OF:			17. LIMITATION OF ABSTRACT	18. NUMBER OF PAGES	19a. NAME OF RESPONSIBLE PERSON
a. REPORT	b. ABSTRACT	c. THIS PAGE			
unclassified	**unclassified**	**unclassified**	**Same as Report (SAR)**	**20**	

(2) Objectives:

The objectives of the present research include development of a suitable CFD solver for solving incompressible flow past airfoils suitable for flying wing micro air vehicle (MAV) design. Suitable airfoils would have to be selected for the purpose. This would be followed by development of a structural analysis solver that would structurally model the airfoil and integrate this solver with the flow solver in order to perform the fluid structure interaction studies for flexible airfoils. Compute flow past selected flexible airfoils and compare their aerodynamic and structural performance with corresponding rigid airfoils. Implementation of smart concept in the structure solver in order to improve the flexible airfoil performance. Perform the fluid structure interaction studies by incorporating smart active layer and explore whether such an embedded layer can improve the aerodynamic and/or structural behaviour of the flexible airfoil. The studies are to be performed over a moderate range of Reynolds number and a fairly wide range of angles of attack to cover a reasonably wide variety of flow conditions. The scope of the project also includes flow solution past three dimensional finite wings with some optimization of the wing planform.

(3) Status of effort:

To achieve the objectives of the present project, the following milestones were achieved sequentially.

- An existing two dimensional structured grid based finite volume Navier Stokes flow solver was modified into an unstructured grid based flow solver. It is capable of solving flow past complicated multi body geometries over low to moderate Reynolds numbers. It was validated on a few benchmark problems successfully before being applied for the present research work.
- The flow solver was used to perform flow simulations on a large number of reflexed airfoils, mainly Eppler series airfoils, which are candidate airfoils for flying wing MAV design. The simulations were performed over moderate range of Reynolds number and angle of attack. The airfoils were assumed to be rigid.
- A finite element based Structural Analysis Solver was developed which would model the structural behavior of the airfoil. The solver was validated on several benchmark problems.
- The smart layer comprising of embedded piezoelectric sensors and actuators was incorporated in the structure solver and was validated on several benchmark problems.
- The fluid and structure solvers were interfaced to compute the fluid structure interaction problem which occurs when considering an elastic wing. Implementation of smart concept in the coupled fluid-structure solver to enhance the aerodynamic and structural characteristics of the airfoil depending on the properties of the embedded piezoelectric sensors and actuators.
- Carrying out fairly large number of flow simulations by considering both rigid and flexible airfoils under uniform and gusty flow conditions. Impact of a sinusoidal gust flow was studied for two different airfoils because MAVs are likely to encounter gusts during flight and their aerodynamic and structural performance may be severely affected in such unsteady environment. For gusty flow simulations two airfoils were considered, namely, Eppler 340 (E340) and a 3% uniform thickness airfoil with same mean camberline as E340.

Certain observations:
From the flow simulation results that were undertaken in the present project it was obvious that the airfoil shape would need to be optimized to obtain optimum aerodynamic performance over a wide range of angle of attack, instead of using existing airfoil shapes. However, such optimization would demand lot more effort and time which could affect achievement of other broad goals of the present research. Therefore it was identified as a study which could be undertaken in future. The existing two dimensional structured incompressible Navier Stokes solver was extended to two dimensional unstructured solver in order to attain desired mesh fineness around airfoil with overall lower number of cells in the computational domain as compared to structured grid case and also to attain the flexibility of using more complex body geometries, including multi element airfoils. However, extension of this solver to three dimensional unstructured NS solver could not be successfully achieved because of considerable complexities which were encountered and which could not be resolved within the time frame of the project. This solver would be developed over the next several months so that it could be used in future to solve flow past finite MAV wing. Investigators would like to work on this development for some more time so that fluid structure interaction studies may later be extended to full three dimensional flexible wing geometries. Also an attempt could be made in optimizing location of smart patches over such a three dimensional wing planform.

(4) Abstract:

A flying wing MAV configuration has several advantages like reduced weight, cleaner aerodynamics, lesser number of control surfaces and actuators, easier attainment of stringent size restrictions as compared to a conventional configuration with tail. However, a tailless wing may not be stable. Therefore, the pitching moment of the airfoil should be low and preferably positive. This could be achieved by reflexed airfoils like Eppler and S series airfoils or low pitching moment airfoils like MH series airfoils. A thin wing could also be considered which has the same mean camber line as that of a conventional airfoil, including the trailing region reflex for the same purpose. Thin wings could be more suitable to facilitate active control and thereby improve the aerodynamic and structural characteristics of the airfoil for widely varying flow conditions. The airfoil could be actively controlled by suitable sensors and actuators. The present paper focuses on numerical investigation of the aerodynamic and fluid structure interaction aspects of a few reflexed and non-reflexed Eppler airfoils as well as thin airfoil of constant 3% thickness and identical mean camberline as that of a reflexed airfoil, namely E340 airfoil. These airfoils could all be potential candidates for a flying wing MAV application. The structural simulation performed by the finite element method is coupled with a finite volume flow solver via a partitioned solution approach. Most published approaches use a partitioned solution scheme, where specialized programs for fluid and structural dynamics are loosely coupled. This approach basically transfers in each time step surface pressure and shear force from the fluid to the surface of the structure and updates the geometry of the fluid domain according to the computed structural displacement. A piezoelectric sensor-actuator layer is embedded within the airfoil in order to improve its aerodynamic and structural response over a wide range of angle of attack. Both a uniform flow at various angles of incidence as well as cosine wave gust has been used to study the steady as well as unsteady characteristics of the airfoil over a modest range of low to moderately high Reynolds number (10^3 to 8×10^4) which is compatible with practical MAV applications. The fluid and structure solvers have been validated independently on certain benchmark problems. Subsequently they have been integrated together for performing the fluid structure interaction studies. For performing the flexible airfoil studies, the three different flexible cases, namely, (i) undamped uncontrolled case (ii) damped case, with natural damping of 2%, and (iii) active control case, i.e., with AFC actuator and PVDF sensor have been considered. The aerodynamic characteristics of rigid airfoils as well as flexible airfoils have been compared. The active control seems to be most impressive in terms of its vibration damping capabilities.

(5) Personnel Supported:

Ph.D. scholars

1. Mr. Atal Bihari Harichandan (working in the AOARD Project since November 2008): working in the area of Aerodynamics. Mr. Harichandan has successfully defended his Ph.D. thesis in October 2010 and has been awarded the degree.
2. Mr. Sharavankumar Basavaraj Kerur (working in the AOARD Project since June 2009): working in the area of aircraft structures, has completed his Ph.D. registration seminar and two years of research.

M.Tech student

1. Mr. Kamanasish Biswas (worked in the AOARD Project from November 2008- May 2009): worked in the area of aircraft structures. Graduated with M.Tech from the Institute in 2009.

** All the above students received regular scholarship from the Institute and topup fellowship from the AOARD project*

(6) Publications:

[1] Harichandan A.B. and Roy A. (2010), Numerical investigation of low Reynolds number flow past two and three circular cylinders using unstructured grid CFR scheme, *International Journal of Heat and Fluid Flow*, Vol 31, pp. 154-171, 2010. (pdf version of the paper enclosed)

[2] Kerur, S.B. and Ghosh, A., Active Vibration Control of Composite Plate Using AFC Actuator and PVDF Sensor, *International Journal of Structural Stability and Dynamics*, Vol. 11(2),2011 (accepted).

[3] Harichandan A.B. and Roy A., CFR: A finite volume approach for computing incompressible viscous flow, *Journal of Applied Fluid Mechanics*, (accepted).
[4] Haldar A., Ghosh. S., Harichandan A.B. and Roy A., Numerical Investigation of Incompressible Low and Moderate Reynolds Number Flow past some Reflexed Eppler Airfoils, *Aerospace Science and Technology*, (under review).
[5] Harichandan A.B. and Roy A., Numerical investigation of flow past two circular cylinders in tandem in the vicinity of a fixed wall. *Journal of Fluids and Structures*, (under review).
[6] Harichandan A.B. and Roy A., Analysis of flows past airfoils at very low Reynolds numbers. *Journal of Aerospace Engineering* (under review).
[7] Harichandan A.B. and Roy A., Numerical prediction of incompressible unsteady flow past three circular cylinders of unequal diameters placed in staggered arrangements, *Journal of Applied Fluid Mechanics*, (under review).

(7) Interactions:

(a) Participation/presentations at meetings, conferences, seminars, etc.

[1] Roy, A. (2008), Numerical Investigation of Low Reynolds Number Flow Past Airfoils for Flying Wing MAV, Proceedings of INDUS-MAV 2008 Workshop held at NAL and ADE, Bangalore, 13-14th Nov., 2008.
[2] Harichandan A.B. and Roy A. (2010), Computation of incompressible flow past array of circular cylinders using an unstructured grid finite volume approach, *Proceedings of the 20th National and 9th International ISHMT-ASME Heat and Mass Transfer Conference*, January 4-6, 2010.
[3] Harichandan A.B. and Roy A. (2010), Flow past reflexed airfoil at low Reynolds numbers, *12th AeSI Annual CFD Symposium*, August 11-12, IISc Bangalore.
[4] Kerur, S.B. and Ghosh, A., Active Control of Geometrically Nonlinear Transient Response of Smart Laminated Composite Plate Integrated With AFC Actuator and PVDF Sensor, *Proceedings of the ASME 2010 Conference on Smart Materials, Adaptive Structures and Intelligent Systems*, September 28 - October 1, 2010, Philadelphia, Pennsylvania, USA, SMASIS2010-3647.
[5] Harichandan A.B., Kerur S.B., Ghosh A. and Roy A. (2010), Fluid structure interaction in airfoils for smart flying wing micro air vehicles, *International Conference on Intelligent Unmanned Systems*, November 3-5, 2010, Bali, Indonesia.
[6] Kerur, S.B. and Ghosh, A., Vibration Control of Geometrically Non-Linear Composite Smart Plate with AFC Actuator and PVDF Sensor, *Proceedings of International Conference on International Conference on Vibration Engineering & Technology of Machinery*, December 13-15, 2010, IIT Delhi, VETOMAC-VI-AB00124 (accepted).
[7] Harichandan A.B. and Roy A. (2010), A numerical study of vortex shedding from two circular cylinders in tandem with ground effect. *Proceedings of the 37th National and 4th International Conference on Fluid Mechanics and Fluid Power*, December 16-18, IIT Madras, (accepted).
[8] Kerur, S.B. and Ghosh, A., Geometrically Nonlinear Transient Response of Active Fiber Composite Smart Plate, *Proceedings of International Conference on Theoretical, Applied, Computational and Experimental Mechanics*, December 27-29, 2010, IIT Kharagpur, India, ICTACEM-2010/257. (accepted)
[9] Harichandan A.B. and Roy A. (2010), Incompressible flow past three circular cylinders of unequal diameters placed in staggered arrangements, *Fifth International Conference on Theoretical, Applied, computational and Experimental Mechanics*, December 27-29, IIT Kharagpur, (accepted).

(b) Describe cases where knowledge resulting from your effort is used, or will be used, in a technology application: None

(8) Inventions:

(a) Discoveries, inventions, or patent disclosures: None

(b) Completed DD Form 882: Enclosed

(9) Honors/Awards: List honors and awards received during the contract period, or emanating from the AOARD-supported research project.

Dr. Arnab Roy: 1) Biographical profile was included in Marquis Who's Who in the World (2009)
2) Nominated as member of IBC (Cambridge, England) Top 100 Engineers (2009)

(10) Archival Documentation:

A MAV flies in a low Reynolds number regime due to its low flight speed and small dimensions. Such flow is often accompanied by laminar boundary layer separation, formation of laminar separation bubble, transition and accompanying low lift-to-drag ratio. The fluctuations in wind speed, which can be comparable to MAV flight speed, make both the instantaneous flight Reynolds number and angle of attack vary substantially and results in an unsteady flight environment. In the present work a few Eppler airfoils have been chosen for investigation. They include Eppler 61 (E61), Eppler 330 (E330), Eppler 334 (E334) and Eppler 340 (E340) respectively. E61 is a non-reflexed airfoil whereas the remaining are reflexed airfoils. Reflex angle (δ) is the negative camber angle found at the trailing edge of reflexed airfoils. The reflex angle of E330, E334 and E340 are δ=5.3º, 2.6º and 6.6º respectively. Uniform flow past these airfoils have been computed for Reynolds number (Re)=10^3, 10^4, 3×10^4, 4.6×10^4 and 8×10^4 respectively at various angles of attack. The essential features of the flowfield have been captured. Pressure contours, streamlines, time averaged airfoil surface pressure distribution, variation of pitching moment with angle of attack and drag polar plots have been included. Uniform flow as well as gusty flow has been solved for E340 airfoil at Re=8×10^4 at various angles of attack by treating the airfoil initially as rigid and later as flexible. Similar flow calculations have been performed for a 3% thick airfoil having same mean camber line as E340 airfoil (henceforth referred to as 3% constant thickness airfoil) at Re=8×10^4 at various angles of attack. The flexible airfoil is constrained at 30% chord for structural calculations. The flow field characteristics and time history of force coefficients for both rigid as well as flexible airfoil cases have been investigated. Time history of the displacement of the trailing edge of the two airfoils were obtained (Figure. 15 &16). Fast Fourier Transform of the trailing edge displacement is used to determine the frequency of vibration of the airfoil. In the present work a loosely coupled approach has been followed for carrying out the fluid structure interaction studies using two different fluid and structure solvers which exchange information back and forth**.**

The Numerical Scheme

The Flow Solver

In order to solve the flow field two dimensional Navier-Stokes equations for incompressible flow in Cartesian coordinates are used, which can be written using indicial notation as follows:

$$\frac{\partial u_i}{\partial x_i} = 0 \qquad (1)$$

$$\frac{\partial u}{\partial t} + \frac{\partial}{\partial x_j}\left(u_j u_i\right) = -\frac{\partial p}{\partial x_i} + \frac{\partial \tau_{ij}}{\partial x_j} \qquad (2)$$

The above governing equations are solved in their non dimensional form in the present flow solver. The constitutive relation between stress and strain rate for a Newtonian fluid is used to link the components of the stress tensor τ_{ij} to velocity gradients. Earlier, a finite volume flow solver was developed based on 'Consistent Flux Reconstruction' (CFR) scheme of Roy and Bandyopadhyay [1] which was originally developed on a structured grid (referred earlier as existing flow solver). Pressure Poisson equation is used for computing the pressure field which gives a divergence free velocity field. In the present work an unstructured triangular mesh based 'CFRUNS' solver has been developed by Harichandan and Roy [2] which is based on the original CFR scheme. This solver is used to compute the flow field around the airfoil. Details of the solver are available in the above reference. The initial unstructured mesh is generated using GAMBIT®. Subsequently when the flexible airfoil shape changes, the flow domain is re-meshed using a suitable moving grid or grid re-meshing procedure based on spring analogy or Master/Slave concept (Lian et al [3]). Since the airfoil is flexible it would deform under the action of air pressure and shear stress acting on its surface from time to time. Since the solver is based on moving grid approach, geometric conservation law is

enforced to ensure consistent flow calculations. A suitable upwinding scheme is incorporated in the solver for enhancing its stability at higher Reynolds numbers (Wu and Hu [4]). The size of the computational domain in terms of airfoil chord length (c) are as follows: length=40c, with 10c distance upstream and 30c distance downstream of airfoil; height=20c, which is equally disposed on top and bottom portions of the airfoil. Approximately 35000 cells have been used to discretise the computational domain. Grid convergence studies have been performed for the CFRUNS solver which are reported in Harichandan and Roy [2]. The following inlet velocity distribution has been used to create gusty flow past E340 airfoil.

$$\begin{aligned} U &= U_0 \\ V &= V_0 \qquad\qquad y>4,\ y<-4 \\ \text{and } V &= V_0 + a\cos(\omega t) \quad -4 < y < 4 \end{aligned} \qquad (3)$$

where U_0, V_0, a and ω are 1.0, 0, 0.8 and $\pi/4$ respectively and y is the distance measured in the direction normal to the flow direction with y=0 located at airfoil mid chord. The time period of a gust cycle is 8 non dimensional time units.

The Structure Solver

Smart materials could be surface bonded or embedded as sensor/actuator layers in the host structure to monitor/ control the behavior of the structure. An Active Fiber Composite (AFC) smart layer which is embedded within an airfoil could be used to monitor and actively control its shape and thereby help in enhancing its aerodynamic performance under varying operating conditions. AFC consists of unidirectional PZT fibres embedded into epoxy matrix and a separate electrode layer with an inter-digital pattern (Bent et al. [5]; Bent and Hagood [6]). In the present investigation in order to solve for the structural response of the smart airfoil to the applied aerodynamic loads a finite element (FE) model has been developed. An eight noded two dimensional quadratic isoparametric element with 5 mechanical degrees of freedom and 1 electrical degree of freedom per node is used to formulate the FE model. The behaviour of smart structure is governed by the equations

$$\{\sigma\} = [Q]\{\varepsilon\} - [e]\{E\} \qquad (4)$$

$$\{D\} = [e]^T \{\varepsilon\} + [\in]\{E\} \qquad (5)$$

A numerical code has been developed based on the formulated FE model. The variable thickness of the airfoil is modeled as a beam of variable thickness. According to the thickness of the airfoil at any chordwise position the element stiffness is calculated separately and finally the global stiffness matrix is assembled. In the present case a graphite/epoxy laminated airfoil is considered. At each calculation step the FE code provides the displacement data for the airfoil surface nodes to the fluid code. The FE code can run both for uncontrolled as well as actively controlled conditions. The actively controlled airfoil results have been obtained based on a constant voltage application. Three different flexible cases have been considered in the present investigation, namely, (i) undamped uncontrolled case (ii) damped case, with natural damping of 2%, and (iii) active control case, i.e., with AFC actuator and PVDF sensor. Based on the displacement data the fluid domain is re-meshed. A moving grid approach is used for this purpose. The fluid code is run till steady state results are obtained for the new shape of the airfoil. The steady state body surface pressure and shear stress distribution is fed back to the FE code to obtain fresh displacement data. This interactive fluid-structure calculations are performed till suitable convergence criteria are satisfied. The time stepping for the fluid and structure solvers have been judiciously chosen to suit the characteristic timescale of relevant physical phenomena.

Results and Discussion

Results of the investigations concerning both rigid and flexible airfoil cases are discussed below. Figure 1 shows the (a) instantaneous pressure contours and (b) streamlines of flow past E340 airfoil at angle of attack (α)=12º, (Re)=10^3. The flow separates from the leading edge of the airfoil and a Von Karman vortex street is formed in the wake of the airfoil. At this Reynolds number the flow is expected to undergo a laminar separation from the leading edge. The Reynolds number is not high enough to trigger a reattachment which will lead to formation of a laminar

separation bubble near the leading edge. Due to negative camber near the trailing edge of the airfoil, the cross-over of pressure distribution occurs on the airfoil surface at moderate angles of attack. This is clearly visible from Figure 2 at $\alpha=8^0$. This crossover phenomenon creates negative lift over portion of the airfoil near trailing edge thereby reducing the overall airfoil lift. However, it is favorable from pitching moment point of view. A fairly extensive study has been carried out on reflexed Eppler airfoils (E325-E339) as a part of the present research which reveals the need for choosing the proper reflex angle to get the correct choice of maximum lift and pitching moment (Roy [7]). Increased reflex decreases the maximum lift coefficient and increases the pitching moment and vice versa. Figure 3(a) and (b) show the pitching moment about quarter chord and drag polar respectively of E330 and E334 airfoils which clearly indicates the effect of variation of reflex angle. Similar studies were also performed on a number of reflexed S series airfoils which indicated comparable findings. E61 is a non reflexed airfoil as mentioned before. The instantaneous streamlines past E61 are shown in Figure 4 for $Re=4.6\times10^4$ at $\alpha=12°$, 15° and 25° respectively. A laminar separation bubble is observed near the trailing edge at α =12° which gradually seems to enlarge with increase in angle of attack. At $\alpha=25°$, the bubble has ultimately led way to a large scale separation and consequent vortex shedding. The time averaged pressure distribution on the airfoil for various angles of attack are shown in Figure 5. The results compare reasonably with those reported in Savaliya et al [8]. All the above studies were performed assuming a rigid airfoil.

For the FE solver, simulations have been initially carried out for 2-D simply supported rectangular plates and the results have been validated for static and dynamic conditions with those available from literature. Using the above code, behavior of cross ply and angle ply laminates has been investigated. Different loadings like uniformly distributed load, impulse load and transverse harmonic loads have been tested. Uncontrolled and active controlled conditions have been simulated. The active control achieved with embedded AFC layer, as expected, gives much more favorable characteristics than the uncontrolled case. Figure 6 is a schematic representation of a rectangular composite plate with AFC actuator layer and PVDF sensor layer. The response of the plate under uncontrolled and active control for impulse load and transverse harmonic load is shown in Figures 7(a) and (b) respectively (Kerur and Ghosh [9]). Figure 8 shows the airfoil laminate arrangement with AFC actuator & PVDF sensor.

Figure 9 shows the instantaneous streamlines and vorticity contours which show the alternate formation of separation bubble on upper and lower surfaces of flexible E340 airfoil under gust for $Re=8\times10^4$, $\alpha=0°$. The flow history is represented from t=32 to 40 time units at interval of one time unit. Careful inspection of the flow field pictures at t=32 and 40 reveals the fact that gust cycle is completed in 8 time units. Figure 10 shows instantaneous streamlines for gust flow past flexible 3% thick airfoil at non dimensional times t=24.0 to 32.0, at interval of one time unit, at $Re=3\times10^4$, $\alpha=12°$. A laminar separation bubble visible on the rear bottom side of the airfoil at t=24.0 vanishes at t=25.0 due to increase in angle of attack. A large separation bubble develops over the upper surface of the airfoil at t=26.0 which enlarges at t=27.0 due to further increase of angle of attack but is still attached to the airfoil surface. At t=28.0 a large eddy structure leaves the airfoil surface and forms secondary eddy structures near leading and trailing edges. At t=29.0 the flow over the upper surface reattaches due to decrease of angle of attack and the shed vortex gets convected into the wake. At t=30.0 an almost streamlined flow is observed over the airfoil. At t=31.0 a laminar separation bubble forms near the leading edge on the bottom surface of the airfoil. This bubble moves to the rear portion of the lower surface at t=32.0. Figure 11 shows lift and drag coefficient history for E340 airfoil in gust flow at $Re=8\times10^4$, $\alpha=0°$. It is noticed that since the inlet is located 10 chord lengths upstream of the leading edge of the airfoil it takes 10 non dimensional time units for it to impinge on the airfoil. As a consequence, the variations in lift and drag coefficients start growing at around that time. The lift force has a time averaged value of zero as $\alpha=0°$. Figure 12 shows the lift and drag coefficient history for 3% airfoil in gust flow at $Re=3\times10^4$, $\alpha=12°$. Figure 13 shows a comparative representation of time varying lift acting on 3% airfoil in gust flow at $Re=3\times10^4$, $\alpha=12°$ for the flexible and rigid cases. It is obvious from the figure that the three different flexible cases show very small difference between each other in terms of their effect on lifting characteristic of the airfoil. However, it is noticed from the figure that there is some difference with the corresponding rigid airfoil case. This makes it obvious that the aerodynamic characteristics of the airfoil does get affected due to its flexibility. The extent of variation would depend on the material properties of the flexible material and the consequent stiffness of the section. Figure14 shows a zoomed view of the lift variation produced on the E340 airfoil for the three different flexible cases. Figure 15 and 16 show the non dimensional deflection of the trailing edge of the airfoil for two different cases. The displacement of the trailing edge is expressed as percentage of the maximum thickness of the airfoil. It is found that the active case is most effective in dampening in the vibrations, more radically for the 3% airfoil case. Figures 17 and 18 show the frequency of vibration of the trailing edge of the E340 and 3% thick airfoils respectively. The frequency spectra are obtained by using Fast Fourier Transform of the displacement time history of training edge

node. The comparatively higher frequency of the E340 airfoil could be linked with its higher stiffness due to higher average section thickness.

Conclusions

A two dimensional unstructured grid based incompressible Navier Stokes solver 'CFRUNS' was developed to perform the present computations for flow past various reflexed and non-reflexed Eppler airfoils, namely, E61, E330, E334 and E340. The initial unstructured grid to discretise the fluid domain was generated using GAMBIT® software. The fluid domain was remeshed whenever necessary by using a moving grid technique accompanied by implementation of geometric conservation law in the solver. Validation of the 'CFRUNS' solver has been reported in Harichandan and Roy [2]. The airfoil flow computations were performed over a range of Reynolds numbers 10^3, 10^4, 4.6×10^4 and 8×10^4 for various angles of attack. In the above simulations the airfoils were assumed to be rigid. Both effect of uniform flow as well as gusty flow past various airfoils was investigated. Instantaneous pressure contours, streamlines, time averaged surface pressure distribution, force and moment coefficients etc were used for performing the necessary analysis. The essential features of the flowfield were captured through the flow simulations. A finite element based smart structure solver was developed as a part of the present research. The solver was validated by applying it on some benchmark problems which are reported in the paper. A loosely coupled fluid structure solver was subsequently developed and applied to solve the fluid structure interaction problem arising in flexible airfoils. Uniform flow as well as gusty flow was solved for flexible E340 airfoil at $Re=8\times10^4$ for various angles of attack as well as 3% thick airfoil at $Re=3\times10^4$. Lift time history have been compared between the rigid and flexible cases. All the flexible cases produce similar lift characteristics but differ to some extent with the rigid airfoil values. The airfoil trailing edge displacement time history reveals that the time varying loading on the airfoil in a gusty situation produces oscillations of the airfoil which could be most effectively dampened by the embedded active piezo layer. The differing trailing edge vibration frequencies could be associated with the varying stiffness of the E340 and 3% thick airfoils. Finally, it was evident from the present study that development of a successful fluid structure interaction model initiates the scope of broader study related to vibration suppression using tailored AFC layers to the shape control of airfoil to improve the in-flight performance of a MAV.

References

[1] Roy, A. and Bandyopadhyay, G., A Finite Volume Method for Incompressible Flows Using a Consistent Flux Reconstruction Scheme, International Journal for Numerical Methods in Fluids, Vol. 52, August 2006, pp. 297-319.

[2] Harichandan A.B. and Roy A., Numerical investigation of low Reynolds number flow past two and three circular cylinders using unstructured grid CFR scheme. International Journal of Heat and Fluid Flow, Vol. 31, 2010, pp. 154-171.

[3] Lian, Y., Shyy, W., Viieru, D. and Zhang, B., Membrane wing aerodynamics for micro air vehicles, Progress in Aerospace Sciences, Vol. 39, 2003, pp. 425–465.

[4] G.X. Wu, Z.Z. Hu, Numerical simulation of viscous flow around unrestrained cylinders, Journal of Fluids and Structures, Vol. 22, 2006, pp. 371–390.

[5] Bent, A.A., Hagood, N.W. and Rodgers, J.P., Anisotropic Actuation with Piezoelectric Fiber Composites, Journal of Intelligent Material Systems and Structures, Vol. 6, 1995, pp. 338-349.

[6] Bent, A.A. and Hagood, N.W., Piezoelectric Fiber Composites with Interdigitated Electrodes, Journal of Intelligent Material Systems and Structures, Vol. 8, 1997, pp. 903-919.

[7] Roy, A., Numerical Investigation of Low Reynolds Number Flow Past Airfoils for Flying Wing MAV, Proceedings of INDUS-MAV 2008 Workshop held at NAL and ADE, Bangalore, India, 13-14th Nov., 2008.

[8] Savaliya, S.B., Praveen Kumar, S. and Mittal, S., Laminar separation bubble on an Eppler 61 airfoil, International Journal for Numerical Methods in Fluids (2009), Published online in Wiley InterScience (www.interscience.wiley.com). DOI: 10.1002/fld.2167

[9] Kerur, S.B. and Ghosh, A., Active Vibration Control of Composite Plate Using AFC Actuator and PVDF Sensor, International Journal of Structural Stability and Dynamics, 2010, (accepted).

Figures

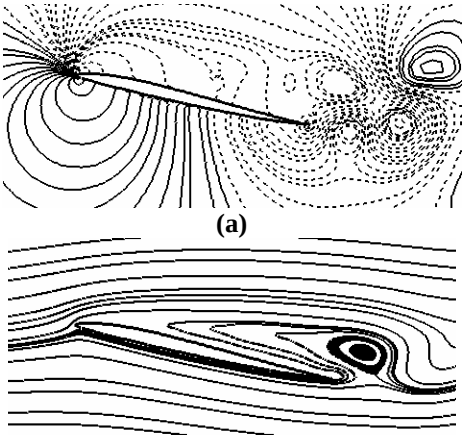

(a)

(b)

Figure 1: Instantaneous (a) pressure contours and (b) streamlines for flow past E340 airfoil at α=12º, Re=10^3

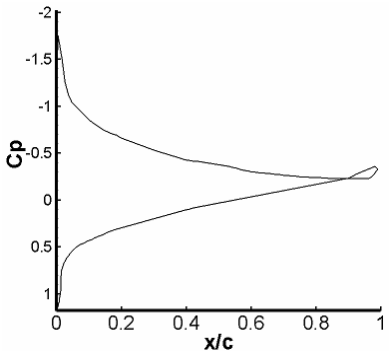

Figure 2: Time averaged surface pressure distribution on E340 airfoil at α=8º, Re=10^3

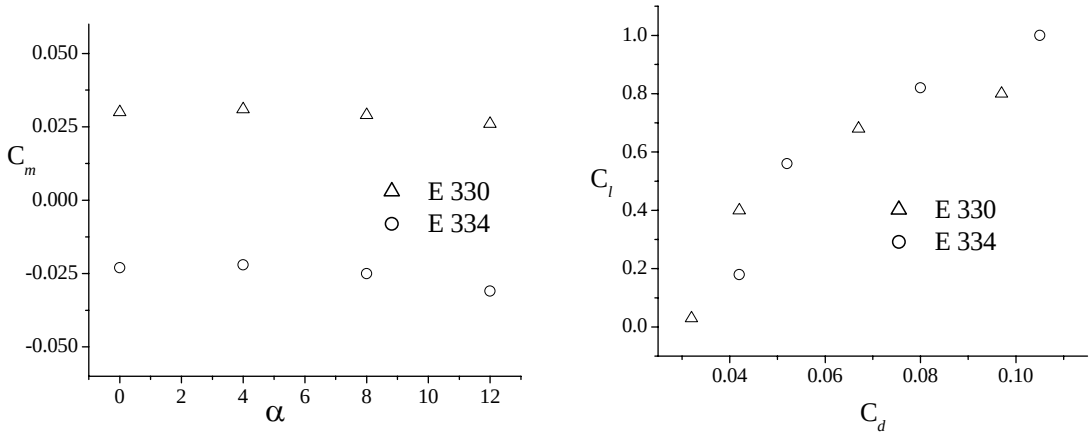

(a) **(b)**

Figure 3: (a) Pitching moment coefficient about quarter chord and (b) drag polar for E 330 (δ=5.3º) and E 334 (δ=2.6º) airfoils at Re=10^4

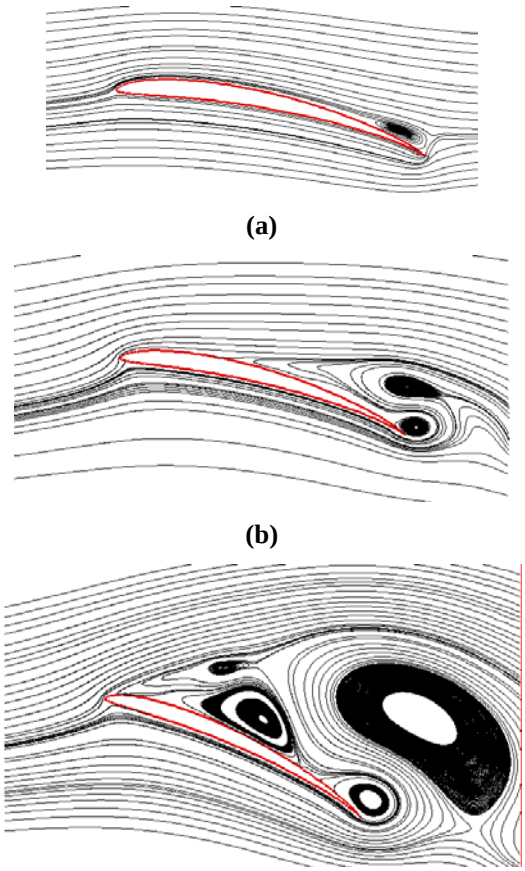

(a)

(b)

(c)

Figure 4: Instantaneous streamlines for uniform flow past rigid E61 airfoil at Re=4.6×10^4, α=(a) 12° (b) 15° and (c) 25° respectively

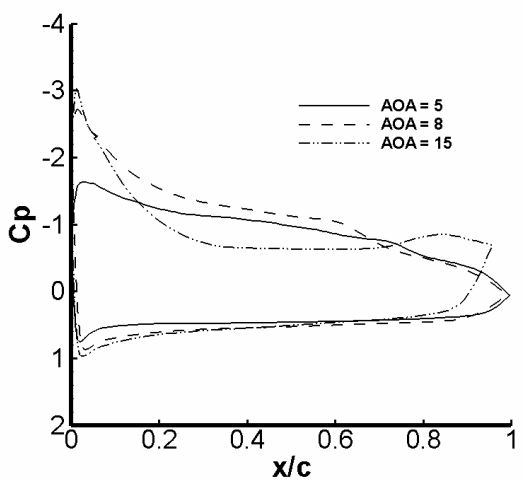

Figure 5: Time averaged pressure distribution on E61 airfoil for uniform flow at Re=4.6×10^4 for various angles of attack

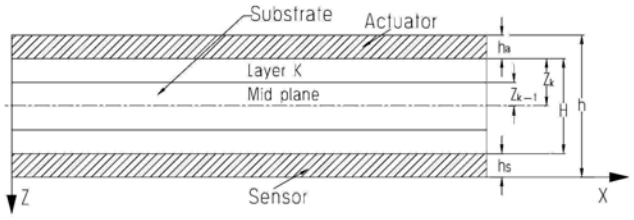

Figure 6: Plate Configuration with AFC Actuator and PVDF Sensor

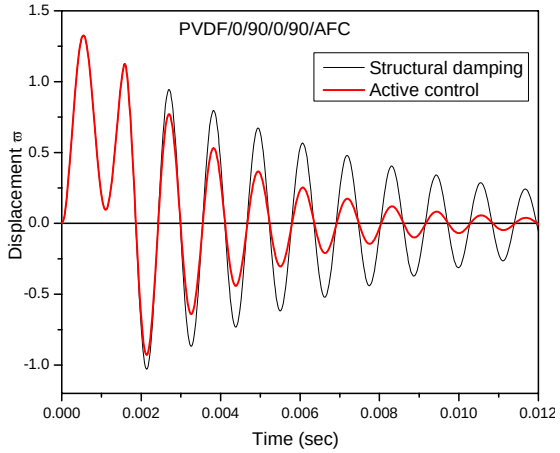

(a)

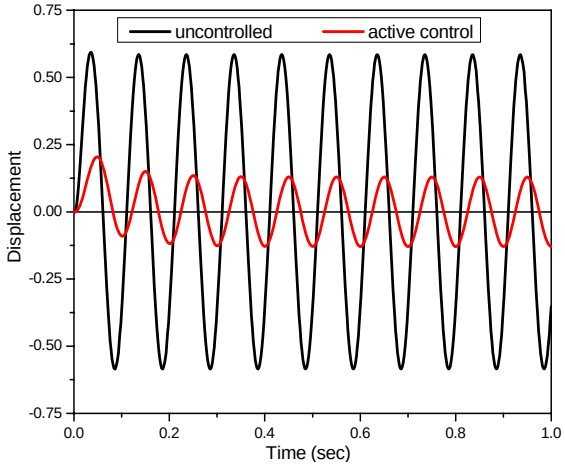

(b)

Figure 7: Uncontrolled and active controlled non-dimensionalised centre deflection of (PVDF/0/90/0/90/AFC) cross ply laminate subjected to (a) impulse load (b) transverse harmonic load

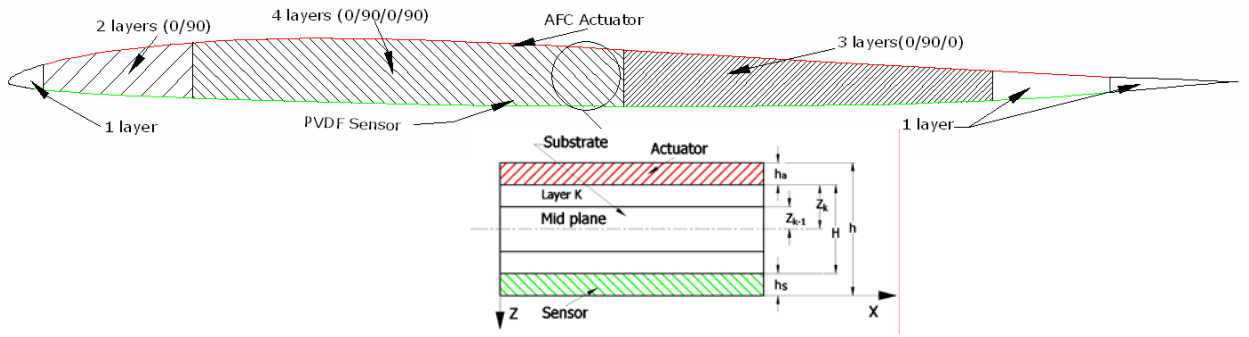

Figure 8. Airfoil laminate arrangement with AFC actuator & PVDF sensor

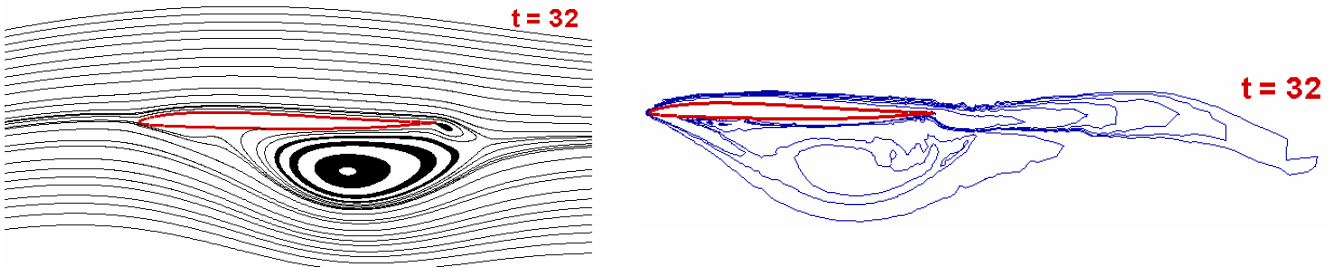

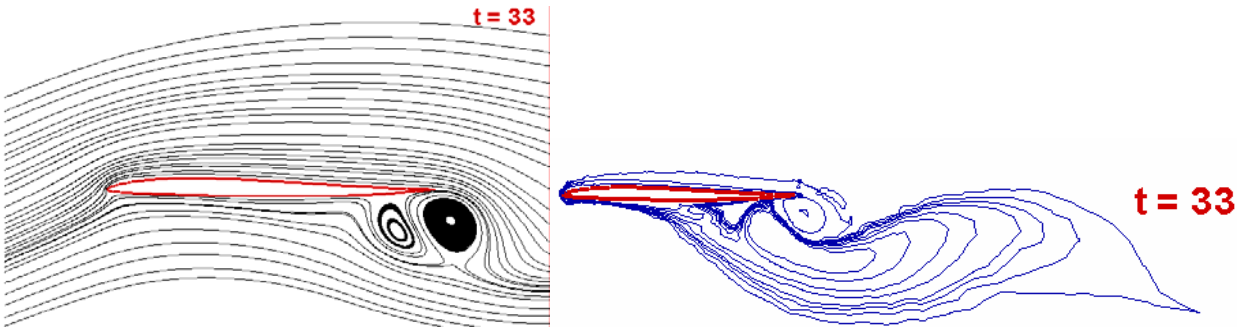
t = 33
t = 33

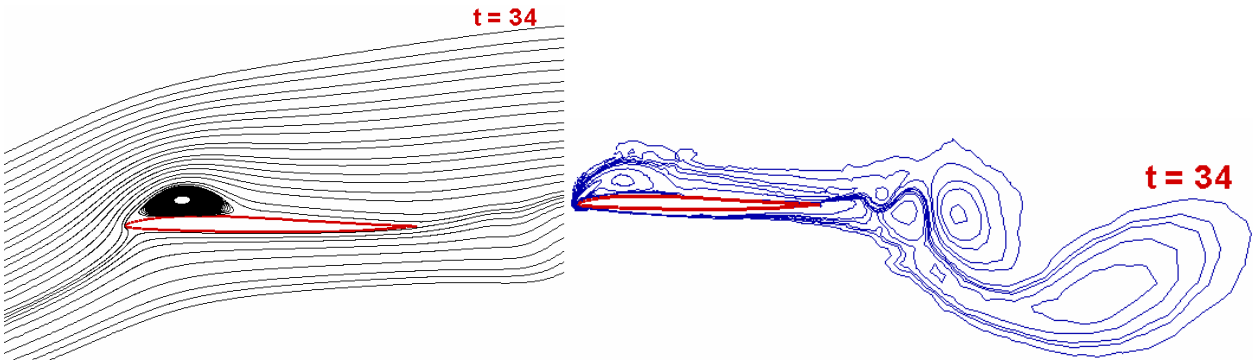
t = 34
t = 34

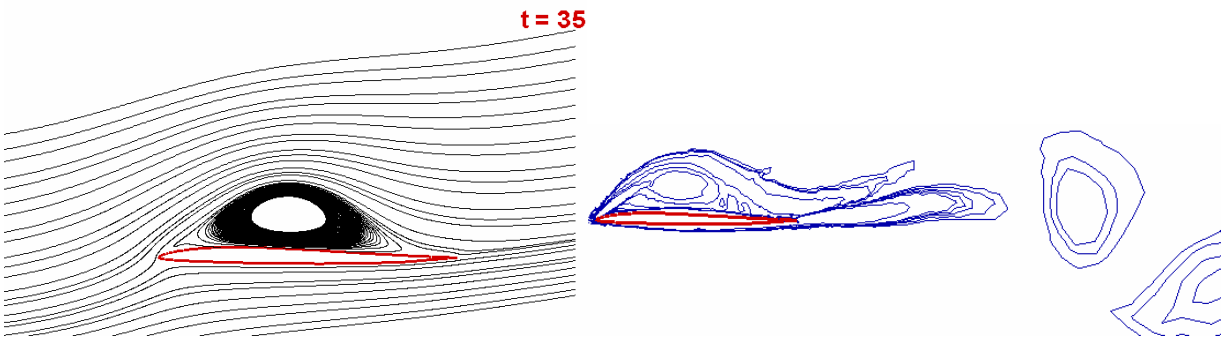
t = 35

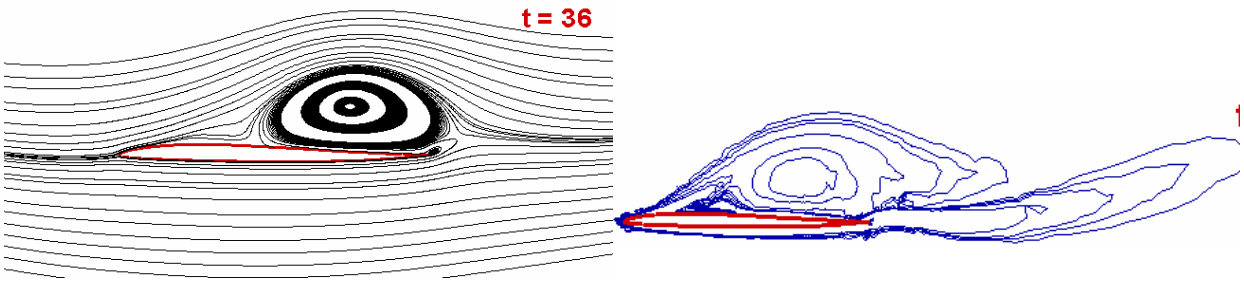
t = 36

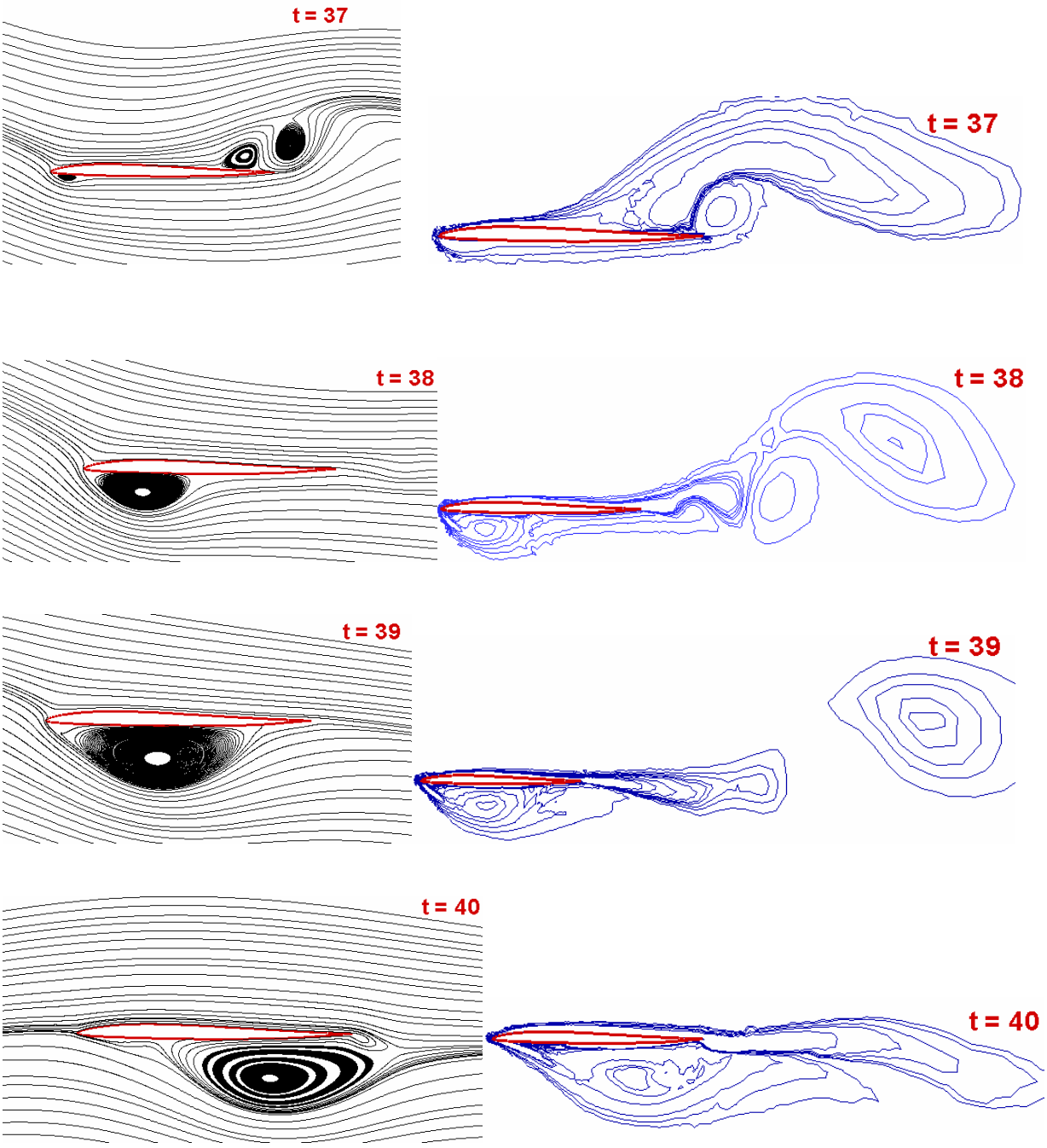

Figure9:Instantaneous streamlines and pressure contours for gust flow past flexible E340 airfoil at non dimensional time t=32.0 to 40.0, at intervals of one time unit, at Re=8×10^4, α=0°

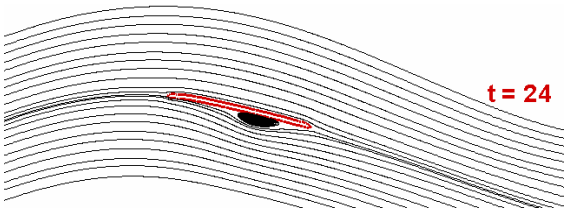
t = 24

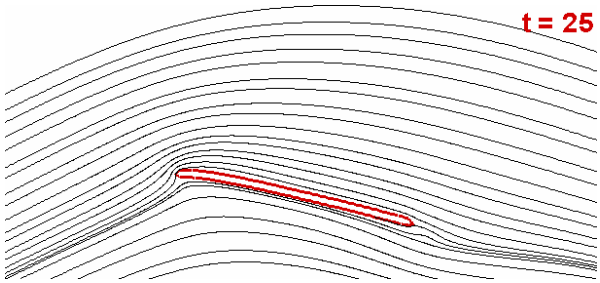
t = 25

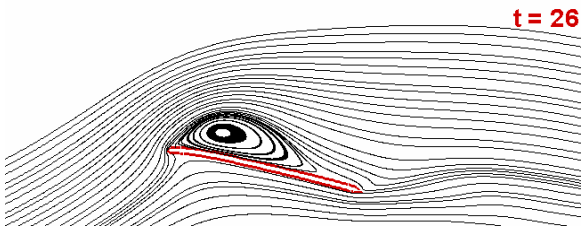
t = 26

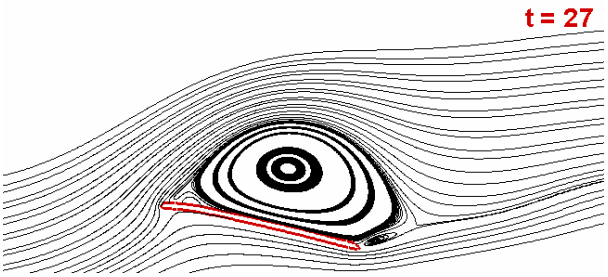
t = 27

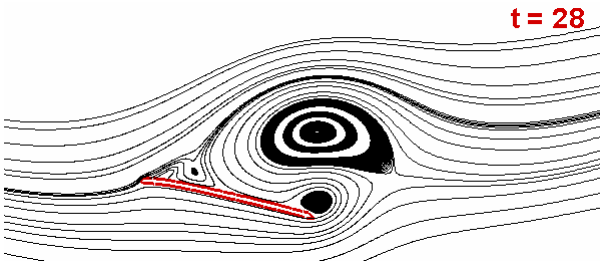
t = 28

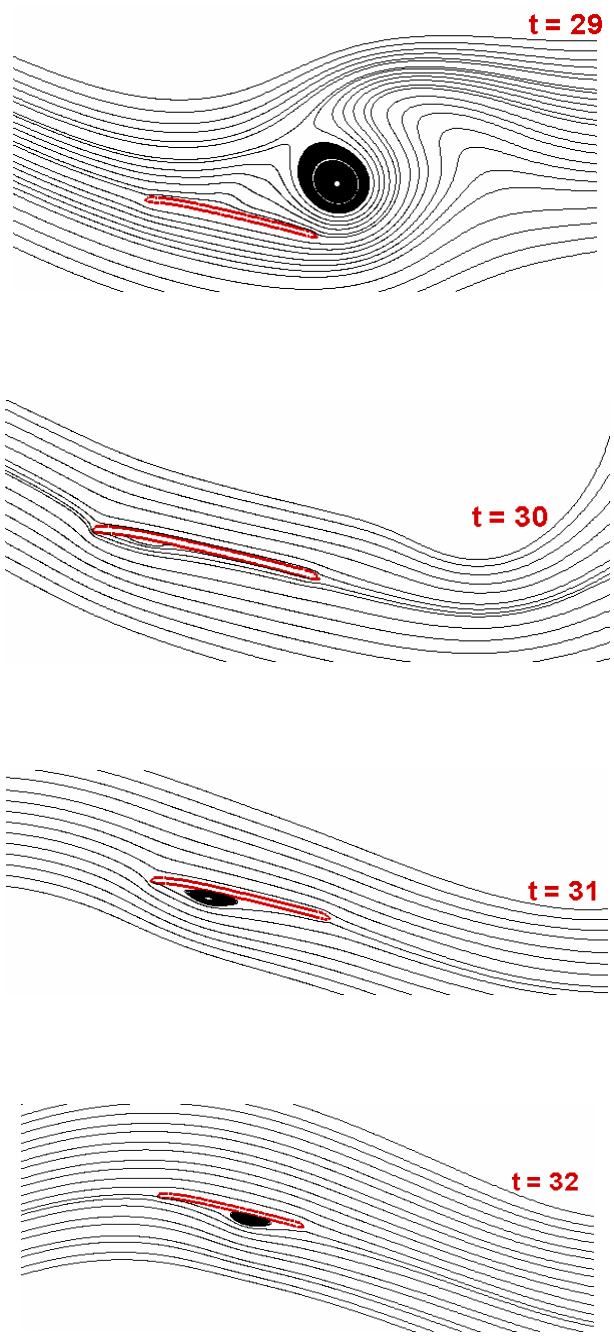

Figure 10: Instantaneous streamlines for gust flow past flexible 3% thick airfoil having same mean camber line as E340 airfoil at non dimensional times t=24.0 to 32.0, at interval of one time unit, at Re=3×10^4, α=12°

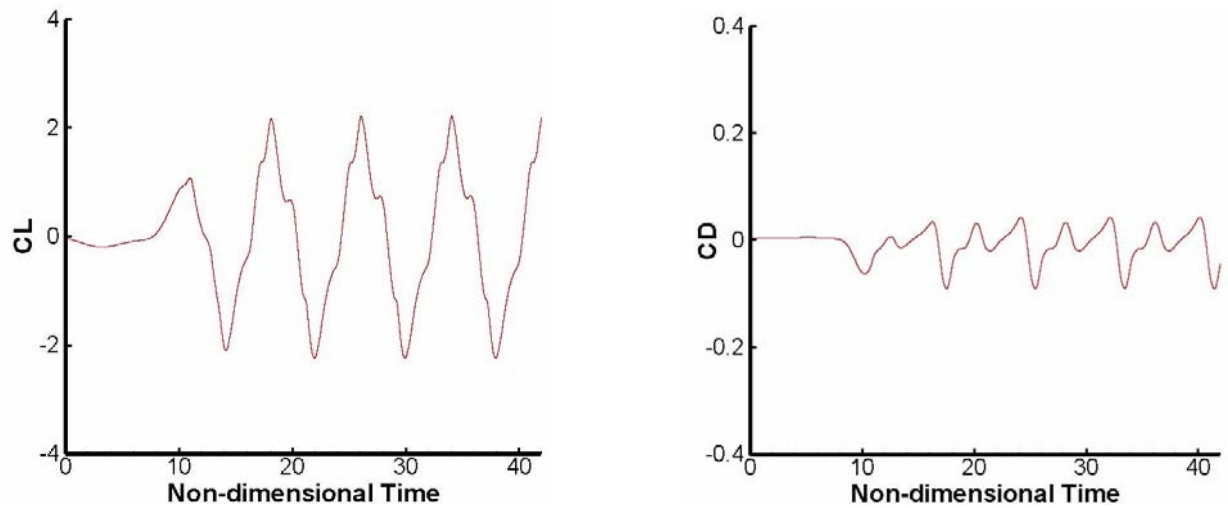

Figure 11 Lift and drag coefficient history for E340 airfoil in gust flow at Re=8×10^4, α=0°

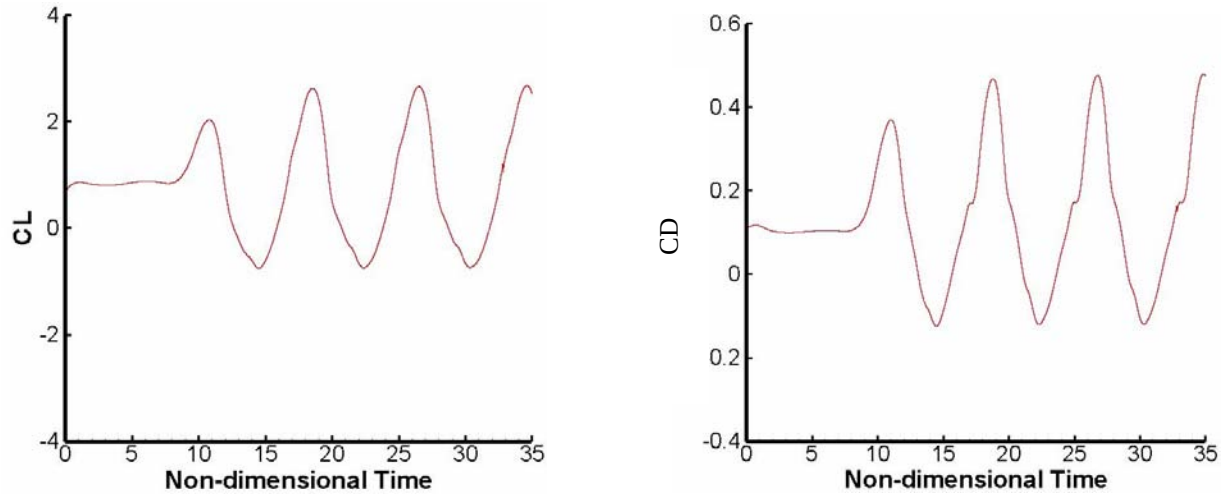

Figure 12 Lift and drag coefficient history for 3% airfoil in gust flow at Re=3×10^4, α=12°

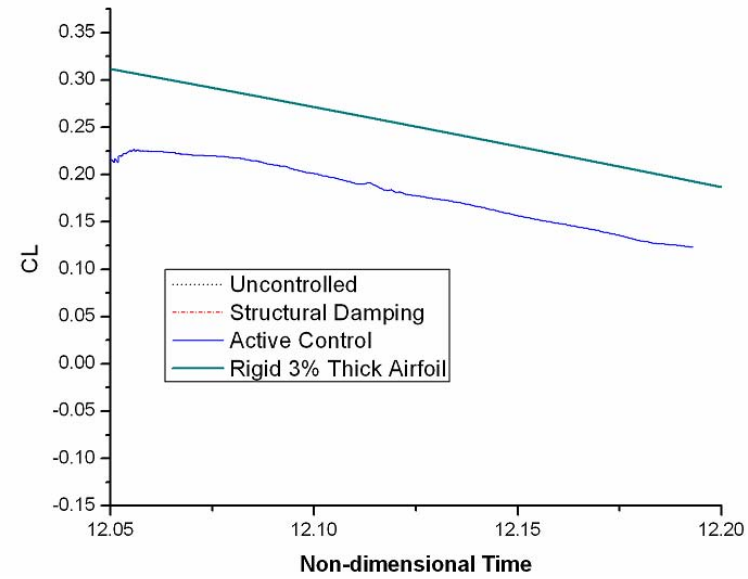

Figure 13 Time varying lift acting on 3% airfoil in gust flow at Re=3×10^4, α=12° for the flexible and rigid cases.

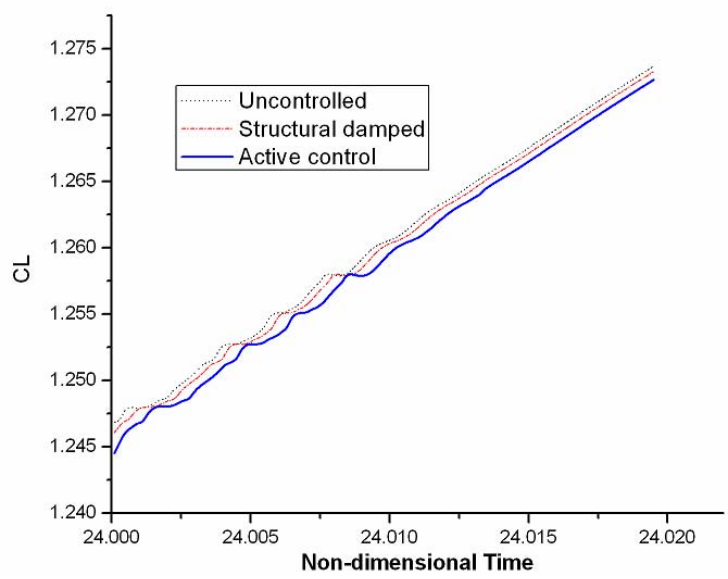

Figure 14 Lift variation produced on the E340 airfoil for the three different flexible cases

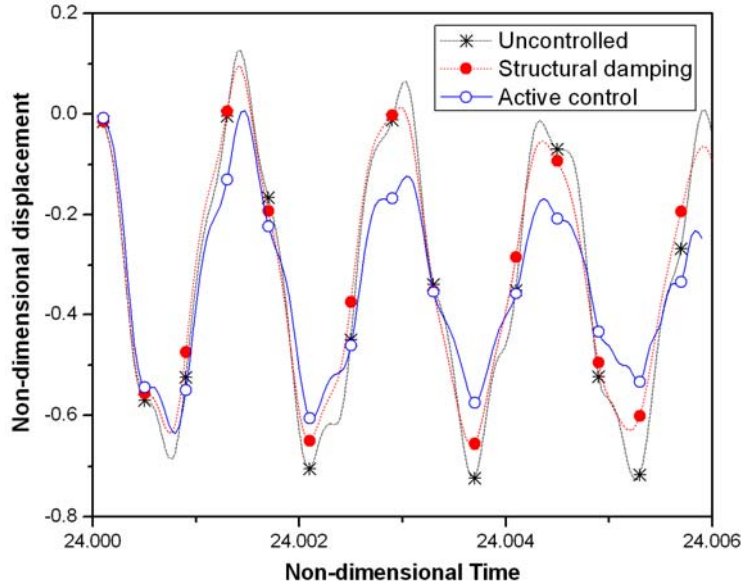

Figure 15 Trailing edge tip deflection for Eppler 340 airfoil for the three flexible cases

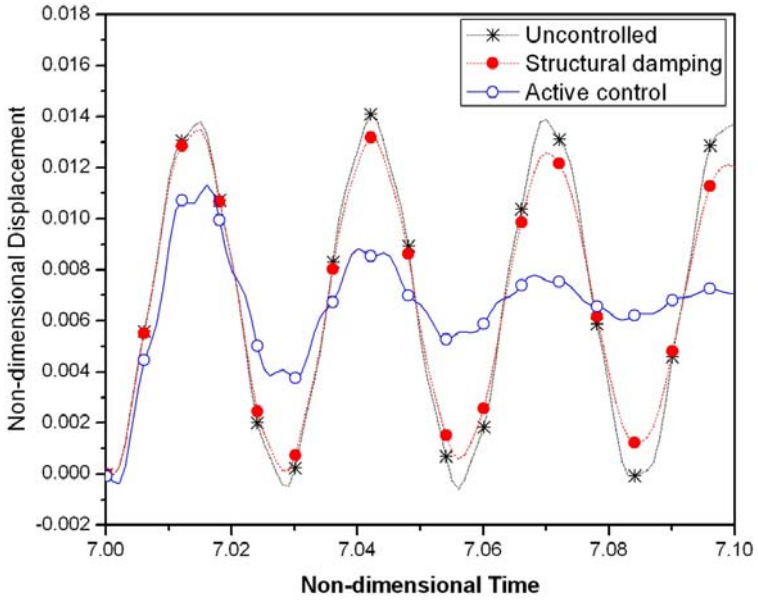

Figure 16 Trailing edge tip deflection for Eppler 340 airfoil for the three flexible cases

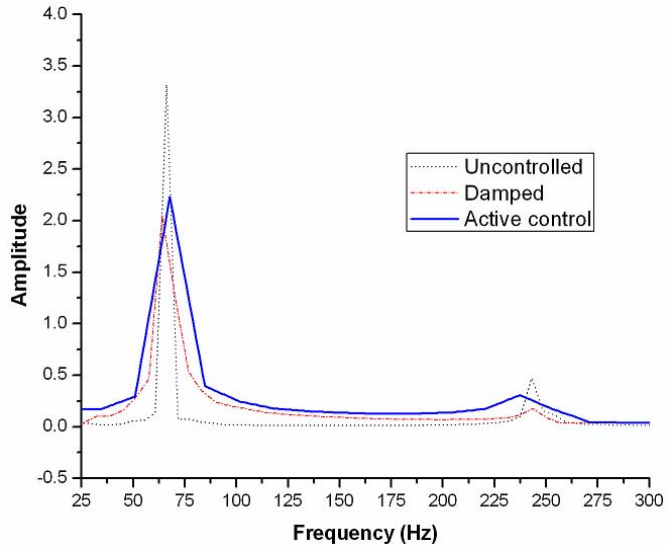

Figure 17 Vibration frequency spectra for Eppler 340 airfoil for the three flexible cases, Re=8×10^4, α=0°

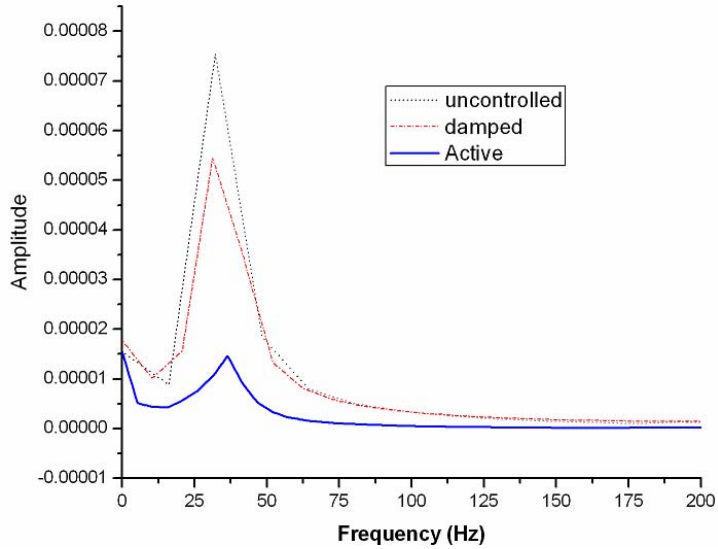

Figure 18 Vibration frequency spectra for 3% thick airfoil for the three flexible cases, Re=3×10^4, α=0°